Heliyon 9 (2023) e20672

Contents lists available at ScienceDirect

Heliyon

journal homepage: www.cell.com/heliyon

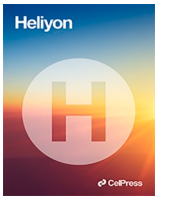

Insights on non-exhaust emissions: An approach for the chemical characterization of debris generated during braking

C. Russo [a], G. Gautier di Confiengo [a], G. Magnacca [b], M.G. Faga [a], B. Apicella [a,*]

[a] Istituto di Scienze e Tecnologie per l'Energia e la Mobilità Sostenibili, CNR, Italy
[b] Dipartimento di chimica, Università degli Studi di Torino, Torino, Italy

ARTICLE INFO

Keywords:
Particulate matter
Ultrafine particles (UFPs)
Brake pad emission
Polycyclic aromatic hydrocarbons (PAH)
Non-exhaust emissions
Nanoparticles

ABSTRACT

Up to 50 % of total $PM_{2.5}$ emissions are due to particles derived from the automotive sector, and both exhaust and non-exhaust emissions contribute to the pollution of urban areas. Fuel incomplete combustion, or lubricant degradation due to high temperatures during the combustion process, are responsible for exhaust emissions. The non-exhaust ones concern brakes, tires and road surface-wear emissions and road resuspension contribution. The present study aims to provide a methodological approach for a detailed chemical characterization of wear friction products by means of a large array of techniques including spectroscopic tools, thermogravimetric analysis (TGA), chromatography, morphological and elemental analysis. The dust sample derived from the wear of a brake pad material was collected after a Noise & Vibration Harshness (NVH) test under loads similar to a Worldwide Light vehicle Test Procedure (WLTP) braking cycle. The TGA shows that only a small fraction is burned during the test in an oxidizing environment, testifying that the sample consists mostly of metals (more than 90 %). Fe exhibits the highest concentrations (50–80 %, even in the form of oxides). Also other kinds of metals, such as Zn, Al, Mg, Si, S, Sn, Mn, occur in small quantities (about 1–2% each). This finding is confirmed by X-ray diffraction (XRD) analysis. The organic fraction of the debris, investigated by means of Raman spectroscopy, has an evident aromatic character, probably due to oxidative phenomena occurring during the braking cycle test. Noteworthy, the extraction of the dust sample with organic solvents, revealed for the first time the presence of ultrafine particles (UFPs), even in the range of few nanometers (nanoparticles), and polycyclic aromatic hydrocarbons (PAHs), recognized as highly toxic compounds. The simultaneous presence of toxic organic carbon and metals makes of concern the non-exhaust emissions and mandatory a deep insight on their structure and detailed composition.

1. Introduction

Traffic-derived air pollution includes both exhaust emissions (a mixture of gaseous pollutants and particulate matter (PM) from fuel combustion and lubricant volatilization/degradation from tailpipe), and non-exhaust emissions, which comprise particles from mechanical abrasion of brakes and tires, erosion of road surfaces and resuspension of a mixture of dust that accumulates on road surfaces, and volatile organic compounds from evaporative loss of fuels and release of solvents [1–3].

* Corresponding author.
E-mail address: barbara.apicella@stems.cnr.it (B. Apicella).

https://doi.org/10.1016/j.heliyon.2023.e20672
Received 15 August 2023; Received in revised form 25 September 2023; Accepted 4 October 2023
Available online 5 October 2023

As regulations undertaken by the government bodies have become increasingly stringent for emissions from engines tailpipe exhaust and technologies have had to adapt, making them increasingly lower, non-exhaust emissions are not regulated yet. Many researchers have found that nowadays both exhaust and non-exhaust emissions contribute almost equally to the increment in airborne PM [4–6]. Moreover, brake-wear emissions were found to be one of the major sources of metal-rich airborne particulate pollution in roadside environments [7].

While much experimental research has been done on the chemical-physical characterization and, consequently, the toxicological and epidemiological impact of exhaust emissions, little is known about non-exhaust emissions. To this regard, of particular concern is the case of brake emissions, due to the heterogeneity of the materials that make up the brakes. It is well known that brakes use friction between a brake pad and a rotating disc to slow or stop a vehicle, by converting kinetic energy into frictional heat. The rotating counterpart has a simpler composition in comparison to brake pads: grey cast iron is the material commonly used.

There are numerous components that made up the brake pad material, and each of them must follow certain parameters that vary according to the conditions of use. Generally, it is required that the coefficient of friction remains constant throughout several operating conditions (varying speed, temperature, and pressure [8]), the rate of wear should be the lowest possible and, finally, the least amount of vibration and noise during braking should be ensured.

Depending on the type and amount of constituents, brake pads can belong to three categories: NAO (Non-Asbestos Organic, 50 % metallic content, phenolic resin, graphite), Low Metallic (Fe 10–50 %, steel and copper), and Semimetallic (more than 50 % Fe and steel fibers) [9].

The constituents of brake pads can be classed as binders, fibers, fillers, and friction modifiers. The binders keep all the materials together and constitute the 20–40 % of the total mass. One of the most widely adopted materials are phenolic resins [10]. Unfortunately, these are not very stable at high temperature, since at 350–400 °C the glass transition occurs and at 450 °C degradation takes place, reducing pad structural integrity [11]. Fibers represent the 5–25 % of the friction constituents [12]. Fibers ensure the structural and thermal stability as well as the wear resistance of the pad. They are usually a mixture of metals (steel or copper), organic materials (Kevlar) or inorganic one (glass, carbon fiber, wollastonite). Fillers can be called functional if they induce thermal and structural stability, and inert if their function is mainly to reduce voids. Finally, abrasives (up to 10 %) [13] increase the friction coefficient and enhance wear resistance (quartz, alumina, zirconia, silicon carbide), while lubricants (5–29 %) [13] reduce the friction coefficient by forming a thin coating, which can also exert a protective function of the pad surface at high temperature (tin sulphide, graphite, molybdenum disulphide, petroleum coke) [14].

During braking, friction between rotating disc and pads always leads to the release of the debris. The wear debris adhere to the pad surface forming an uneven friction layer, mainly constituted by oxidized metals (iron oxides are the major components), fragments of carbonaceous matter and degradation products of phenolic resins [15]. Mechanical wear usually leads to the release of large particles with sharp edges, belonging mainly to PM_{10} (PM $<$ 10 μm) or $PM_{2.5}$ (PM $<$ 2.5 μm) categories. Oxidative wear generates submicron-sized particles, even in the nanometric range (ultrafine particles (UFPs) less than 30 nm [16], organized in clusters of spherical particles, by degradation of organic binder with subsequent condensation and agglomeration of these finest fractions. The latter are mainly made up by amorphous carbon, graphitic particles, and various metal-based components. The finest particles were observed to be attached to the surface of larger particles [17].

These airborne particles released into the air can easily be inhaled, and the high metal content results toxic for human health. Moreover, Gasser et al. [18] evaluated the toxicological effects of brake wear particles on human epithelial cells and found that particles damage the cells increasing oxidative stress and causing a pro-inflammatory cell response after 24 h exposure.

In this framework, in the present work it is reported a methodological approach for a detailed chemical and morphological characterization of wear particles released from brake pad systems collected at the end of the NVH (Noise & Vibration Harshness) braking test (with conditions similar to a WLTP, Worldwide Light vehicle Test Procedure braking cycle) by using an array of analytical techniques. In particular, morphological and compositional information was given by FESEM (Field emission scanning electron microscopy) analysis and thermogravimetry. Raman spectroscopy and XRD (X-ray diffraction) were used to characterize the carbonaceous solid part, whereas size exclusion chromatography, UV–Visible and Fluorescence spectroscopy were performed to get insights on the size distribution of UFPs and on the composition of the soluble organic fraction (SOF). Only one exemplary sample was analyzed and it was not collected in the aerosol but directly on the pad using a brush to gently clean all pad surfaces and to remove only the friction layer, which is representative of the particulate emitted in the environment from the pad. In this way, it is possible to collect enough material to set-up the analytical approach, which can then be applied on the analogous particulate emitted from the pad and collected in air on filters. This approach will be useful in a next work for a rapid screening of the particulate composition as a function of the composition of the pad. It is reasonable to assume that the particulate on the friction layer presents a very similar size distribution with respect to the debris in air just near the brake.

The coexistence of metals and highly toxic organic compounds found in debris in the present work raises questions about non-exhaust emissions and necessitates a thorough understanding of their detailed structure. In particular, it is of concern that, as found here for the first time, metals and organic fraction are linked together in the particulate, and the organics are mainly constituted by dangerous aromatic species. Moreover, organic particulate is present also in nanometric and, therefore, much more toxic particles.

2. Experimental setup

2.1. Samples

The wear particles under investigation were collected using a brush to gently clean all pad surfaces and to remove only the friction

layer (pad: RCM625B4A; disc: GJL150, cast iron alloy). The collected powder was divided in 3 samples, in order to repeat all the measurements 3 times for verifying the homogeneity and reproducibility of the sample. Reproducibility was found to be around 10%.

Each debris sample was characterized by FESEM images with EDS, thermogravimetry and Raman spectroscopy. A small amount of debris was washed with dichloromethane (DCM) for separating the organic compounds, soluble in DCM, from the insoluble solid fraction present in the dust. The SOF was then subjected to spectroscopic (UV–Visible absorption and fluorescence) and SEC analysis.

2.2. Analytical techniques

2.2.1. Thermogravimetry

TGA experiments were carried out on a Perkin–Elmer Pyris1 Thermogravimetric Analyzer. About 3 mg of sample were heated from 50 to 900 °C at a rate of 10 °C min^{-1} in oxidative environment (air, 30 *mL* min^{-1}).

2.2.2. FESEM images EDS analysis

A Field Emission Scanning Electron Microscope Tescan S9000G, (FESEM), Schottky emitter, equipped with Secondary and Electron Backscatter Diffraction Detector (SE and EBSD) and microprobe for elemental analysis, was used. The instrument has a resolution of 0.7 nm (at 15 keV with In-beam SE detector).

2.2.3. XRD

XRD spectra were acquired on a Bruker D2 II with Cu Catode (Kα1 1.54 Å, 30 kV voltage and 10 W power; 0.1° slit divergence e 1.5° Soller slit). A Ni filter was employed for removing Kβ (λ = 1.392 Å) X-ray spectral lines of copper. Instrument resolution: 0.05° 2q. The holder is a "Zero background holder " in silicon crystal.

2.2.4. Raman spectroscopy

Raman spectra were measured using a Horiba Xplora Raman microscope system (Horiba Jobin Yvon, Japan) with an excitation wavelength of λ = 532 nm (frequency doubled Nd: YAG-solid state laser, 25 mW). The microscope was focused onto the sample surface using the objective with 100X magnification. Raman spectra were recorded in the range of 500–3500 cm^{-1} (Raman shift). Acquisition time was set at 30 s. Raman spectra have been acquired in six different measuring points and an average spectrum was calculated to account for sample heterogeneity.

2.2.5. UV–visible and fluorescence spectroscopy

UV–Visible absorption and fluorescence emission spectra of the SOF were acquired on DCM solutions using a 1-cm path-length quartz cuvette. A Fluoromax spectrofluorometer (Horiba Scientific) and a V-770 UV–Visible/NIR spectrophotometer were used to measure the steady state fluorescence and the absorption spectra, respectively.

2.2.6. Size exclusion chromatography

Size exclusion chromatography (SEC) of the SOF was also performed on a highly cross-linked "individual-pore" column (Polymer Laboratories, Ltd., U.K.; particle size of 5 m diameter and a pore dimension of 50 nm). The injection volume was 100 µl, and the analyses were carried out at a flow rate of 0.5 ml/min at a temperature of 70 °C. The chromatogram was obtained by fixing the absorption wavelength at 370 nm of an HP1050 UV–Vis diode array detector, measuring the absorption spectra in the 250–600 nm wavelength range. The molecular weight (MW) calibration of the column was obtained by measuring the elution time of polystyrene and polycyclic aromatic hydrocarbons (PAH) standard species of known MW [19,20].

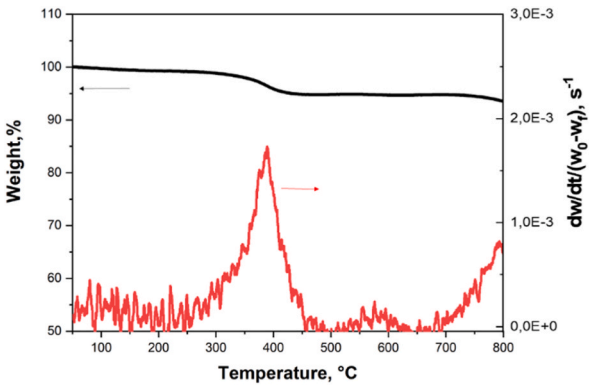

Fig. 1. Thermogravimetric analysis (TGA) (in black) and differential thermogravimetric curves (DTG) (in red) profiles of debris sample.

3. Results and discussion

The data obtained from TGA in oxidative environment are shown in Fig. 1. The trend of the oxidation curve is constant up to 350 °C, when the organic constituents begin to burn. The TGA profile and its derivative (differential thermogravimetric curves, DTG) indicate that the only mass loss recorded was due to the oxidation of the organic fraction present in the debris, which amounts to about 8 %. Therefore it is hypothizable that the matrix of this sample is mainly metallic and thus it remains as residue at the end of the oxidation run.

Fig. 2 represents characteristic FESEM images of the frictional dust. According to Kukutschová's findings [17], the smallest particles are "attached" on the largest particles surfaces, increasing the danger of these airborne particles. In fact, the larger fraction can access the human body through respiration or ingestion, taking with it the smaller fraction, which can be released, reaching also other organs and damaging the organism [21,22]. The elemental composition of the sample was evaluated by Energy Dispersive Spectroscopy (EDS) analysis and the results are summarized in Table 1. The acquisitions were made in six different locations of the sample to account for the sample heterogeneity. Two peculiar areas that differ from each other by the amount of Fe detected were identified. A zone with a poorer content of Fe (50–55 wt%), probably in the form of iron oxides [17], based on the presence of O amounts to 20–30 wt%, with a higher concentrations of C (10–15 wt%), was observed. To the remaining percentage other metals participate as Zn, Al, Mg, Si, Sn and S with a value around 1–2% for each. The EDS analysis also detects other areas with higher amounts of Fe (80-85 wt%), with a smaller component of O (5 wt%) and C (5 % wt%). The other metals participate, however, with a value still around 1–2 wt%. Table 1 reports the average values between these areas for the most frequently detected elements.

An example of the distribution of elements in a representative area of the specimen is shown in the rigth part of Fig. 2. The dominant presence of oxygen and iron is evident, interspersed with micrometer-sized sheets of carbon. The extensive presence of Fe and O precludes the observation of metals present in significantly smaller amounts, except for zinc, whose presence is detected. The Fe/O ratio is consistent with the massive presence of iron oxide, that can arise from steel oxidation as a consequence of braking [23].

The results obtained from the thermogravimetric analysis are confirmed by the EDS: the organic fraction (both volatile organics and graphitic-like particles) represents less that the 10 wt% of the sample (total percentage of carbon). All the remaining material is composed of metals and metal oxides, constituting the residue of the thermogravimetric test.

In Fig. 3 the XRD spectrum of the sample is reported. All the peaks are sharp and can be attributable to metallic oxides, for comparison with the library. The metallic oxides peaks are also superimposed and partially cover the carbon matrix peaks, typically located at 26–27° and 42–44° [24,25].

The Raman spectrum, reported in Fig. 4, was acquired in the first order range, 900–1900 cm^{-1} and deconvolved using a five-bands procedure that have been optimized for soot samples [26]. It allows to draw out the contribution of peaks at around 1600 (G-band), 1500 (D3-band), 1270 (D4-band) and 1325 cm^{-1} (D-band). The intensity of D-peak is related to the breathing mode of aromatic rings in disordered structures, while the intensity of G-peak is related to the streching of sp^2 carbon bond [27].

The ratio betwenn the D and G peak intensity, I(D)/I(G), is the main parameter used to quantify order and disorder in the carbon materials analysis [27]. This ratio was calculated as 1.2, value that corresponds to a good level of nanostructural order and to a graphitic-like structure [26]. Through the well-known Equation: $\frac{I(D)}{I(G)} = C(\lambda) * {L_a}^2$ [27] it has been possible to estimate an aromatic layer size, La, of 1.36 nm. The used equation is valid for disordered materials as soot, constitued by aromatic clusters of few nanometers [27].

The presence of these carbonaceous particles could be due to the oxidative wear of the organic compounds belonging to the binder of the original brake pad. These particles, coming from the degradation of the organic binder, undergoes oxidation due to high temperature reached during the braking test.

The oxidative nature of the friction processes during braking was previously proven by contrasting the initial friction composite with its non-airborne wear particles recovered during brake dynamometer experiments [28].

Raman spectroscopy gives information only on the solid carbonaceous particles, then an extraction procedure with DCM was

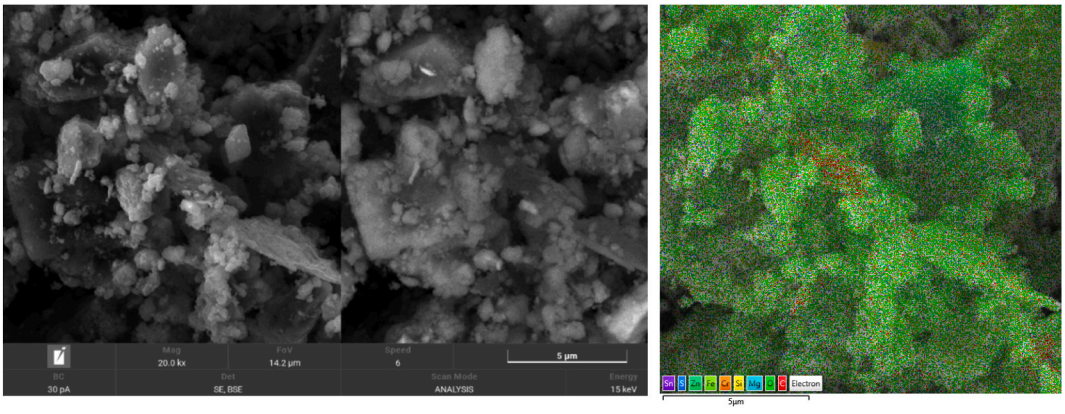

Fig. 2. Field emission scanning electron microscopy (FESEM) images of debris surface without (left) and with element distribution (right).

Table 1
Weight and atomic percentages of elements detected by Energy Dispersive Spectroscopy (EDS) analysis of debris sample.

	wt%	at%
Fe	62	32.7
O	20	36.9
C	10	24.6
Zn	2	0.9
Al	1	1.1
Mg	1	1.2
Si	1	1.1
Sn	2	0.5
S	1	0.9

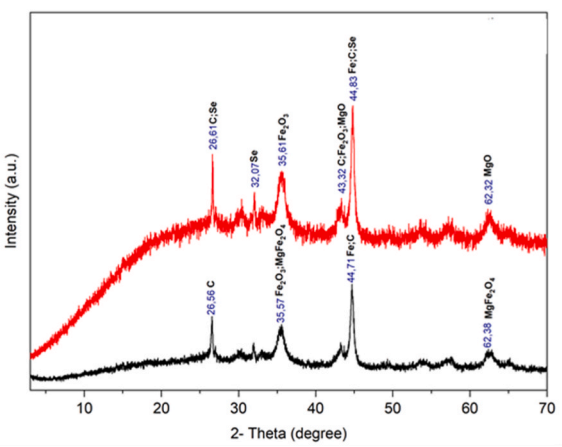

Fig. 3. X-ray diffraction (XRD) spectrum of debris sample (in red, as aquired; in black after fluorescence subtraction).

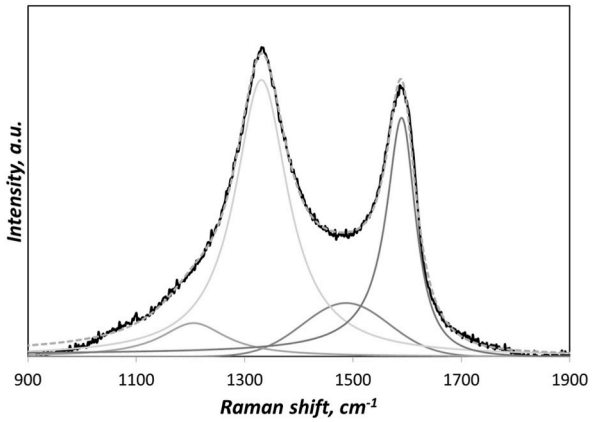

Fig. 4. Raman spectrum of the debris sample along with the deconvoluted peaks.

performed to analyse in details also the SOF. The optical properties of the SOF derived from debris are summarized in Fig. 5: the UV–Visible absorption spectrum (left panel), the steady-state fluorescence spectrum excited at 350 nm (central panel) and the contour map of the 3D fluorescence spectra (right part). The emission and absorption spectra exhibit some fine structure suggesting the presence of PAH. Even if the concentration of these species is low (order of pg/L), as demostrated by the fact that they are detectable only by spectroscopic techniques but not by GC-MS of DCM extract (not reported here for sake of brevity), their presence is of concern as PAH are known to be mutagen and carcinogen [29] also at so low concentrations.

Moreover, the absorption tail in the visibile [30] and an emission peaked at relatively high wavelengths (around 480 nm) also indicate the presence of higher MW aromatic species in the solution [31], which can be even more toxic than PAH. The region of fluorescence emission maximum is localized beetween 450 and 500 nm (red region in the contour map), a typical range of fluorescence

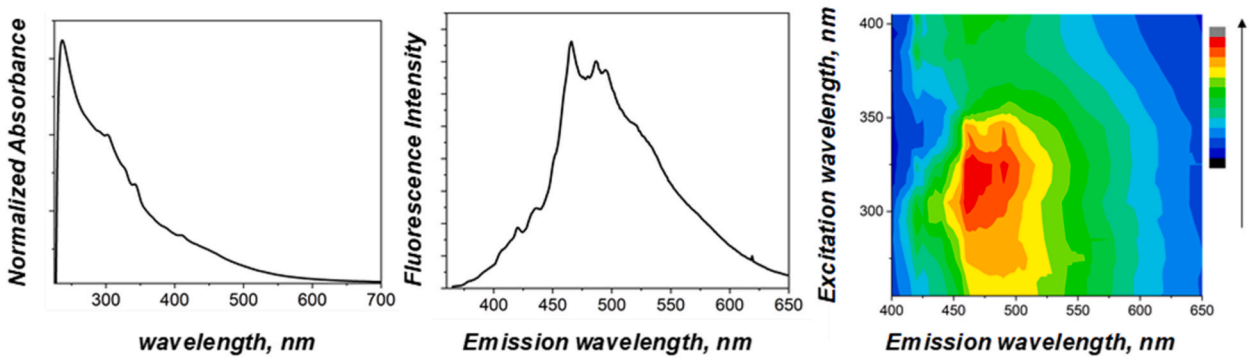

Fig. 5. Steady-state fluorescence spectra (central part), the contour maps of the 3D fluorescence spectra (right part), and through UV–Visible absorption (left part) of the soluble organic fraction (SOF) derived from dichloromethane (DCM) washing of the debris sample.

of organic carbon from high temperature processes of carbon precursors [32].

The synchronous fluorescence spectrum of the SOF shown in Fig. 6 makes this finding even clearer. Indeed, it is possible to distinguish between different classes of different-sized polycyclic aromatic hydrocarbons (PAHs) using the synchronous fluorescence technique, which involves simultaneously scanning the excitation and emission wavelengths using a $\Delta\lambda = 10$ nm [33]. The synchronous fluorescence of the SOF confirms the presence of PAH from 3 to 7 rings, as well as of bigger PAH not detectable by GC-MS, in accordance with the absorption and emission features (Fig. 5).

The MW distribution of the SOF was evaluated, drying the samples in DCM and dissolving them in NMP for SEC analysis and reported in Fig. 7. It is observable that more than the molecular species (with very low signal), particles of nanometric dimensions (assuming density of 1.2 g/cm^3) are present. The reliability of SEC technique for the detection of nanoparticles have been assessed in our previous works [19,34,35].

The possibility of particle fragmentation for the formation of nanoparticles has been ruled out because the only pre-treatment made on the particulate was the solvent extraction.

The presence of UFPs smaller that 30 nm in brake pad particulate was recentely demonstrated [16] and this is particularly important for their neurotoxic potential.

The results of the present paper, which show the presence in the debris of high MW aromatic structures, nanoparticles and graphitic-like carbon particles, typically formed in oxidation/pyrolisys process from light organic compounds, suggest that these species can be formed via evaporation and condensation wear mechanisms of carbonaceous components of a friction composite.

The simultaneous presence of organic compounds identified as highly toxic [29,36], UFPs and metals demonstrated by the present paper makes of concern the non-exhaust emissions and mandatory a deep insight on their structure and detailed composition.

4. Conclusions

A NVH braking test, with loads similar to a WLTP braking cycle, was made on a RCM625B4A pad with a cast iron alloy disc to collect wear particles released from brake pad systems using a brush to gently clean all pad surfaces and to remove only the friction layer. A thermogravimetric test in air environment and an EDS analysis of the collected powder have allowed quantifying the metals and organic components present in the sample. An average percentage less than 10 % was estimated to account for the organic fraction present in the sample, whereas the rest is mainly constituted of iron and iron oxides and, in a smaller percentage, of other metals belonging to the inorganic matrix of the pad. XRD confirms the high presence of metals with respect to carbon matrix. In addition, FESEM images show that smallest particles, probably derived from oxidative wear, are “attached” on the surface of the largest ones. The breathing of these submicron-sized particles could increase their impact on human health. The graphitic-like characteristic of the organic particles was demonstrated by the structural parameters derived from the Raman spectroscopy analysis, indicating that this small fraction comes out from an oxidative process (high temperature during the braking test). The DCM extract of the debris powder, representing the soluble organic fraction, was analyzed by fluorescence and absorbance spectroscopy and size exclusion chromatography. The results evidenced, for the first time, the presence of PAHs and UFPs in the soluble organic fraction, further increasing the toxicological effects.

The coexistence of metals and highly toxic organic compounds found in debris in the present work is of concern and raises questions about non-exhaust emissions and necessitates a thorough understanding of their detailed structure.

Funding statement

This research did not receive any specific grant from funding agencies in the public, commercial, or not-for-profit sectors.

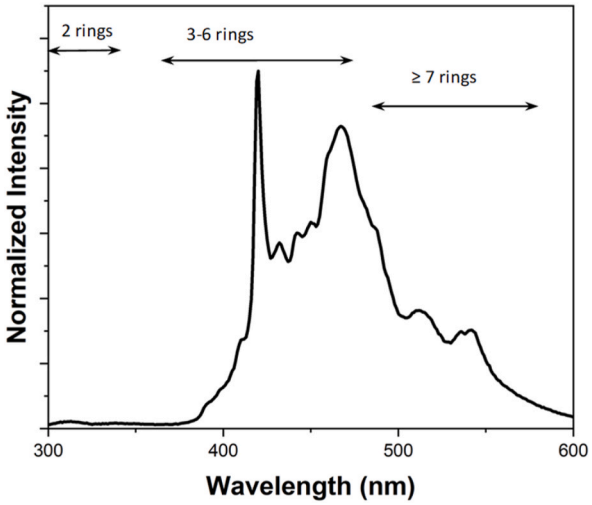

Fig. 6. Height normalized synchronous fluorescence spectrum ($\Delta\lambda = 10$ nm) of the soluble organic fraction (SOF) derived from dichloromethane (DCM) washing of the debris sample.

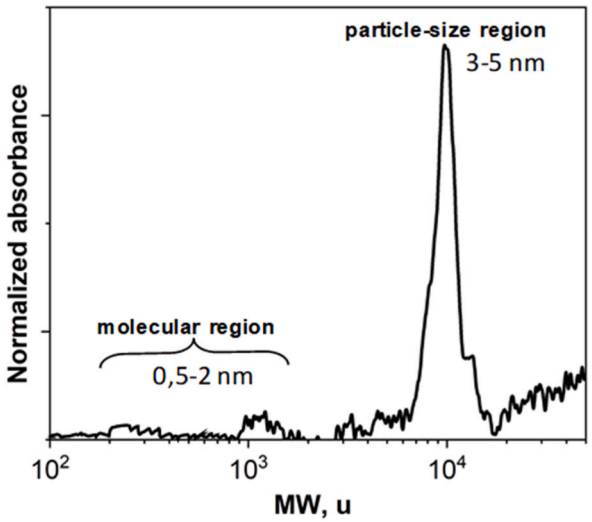

Fig. 7. MW distribution profile acquired from size exclusion chromatography (SEC) of the soluble organic fraction (SOF) derived from dichloromethane (DCM) washing.

Data availability statement

Data will be made available on request.

Additional information

No additional information is available for this paper.

CRediT authorship contribution statement

C. Russo: Conceptualization, Data curation, Formal analysis, Investigation, Writing – review & editing. **G. Gautier di Confiengo:** Conceptualization, Data curation, Formal analysis, Investigation, Writing – review & editing. **G. Magnacca:** Conceptualization, Data curation, Formal analysis, Investigation, Writing – review & editing. **M.G. Faga:** Conceptualization, Data curation, Formal analysis, Investigation, Writing – review & editing. **B. Apicella:** Conceptualization, Data curation, Formal analysis, Investigation, Writing – original draft, Writing – review & editing.

Declaration of competing interest

The authors declare that they have no known competing financial interests or personal relationships that could have appeared to influence the work reported in this paper.

Acknowledgements

All authors acknowledge RAICAM Industrie S.r.l. for kindly providing the samples.
Dr. Francesca Cerciello from Ruhr-University Bochum has been acknowledged for her help in XRD acquisition.

References

[1] A. Piscitello, C. Bianco, A. Casasso, R. Sethi, Non-exhaust traffic emissions: sources, characterization, and mitigation measures, Sci. Total Environ. 766 (2021), 144440, https://doi.org/10.1016/j.scitotenv.2020.144440.
[2] R.M. Harrison, J. Allan, D. Carruthers, M.R. Heal, A.C. Lewis, B. Marner, T. Murrells, A. Williams, Non-exhaust vehicle emissions of particulate matter and VOC from road traffic: a review, Atmos. Environ. 262 (2021), 118592, https://doi.org/10.1016/j.atmosenv.2021.118592.
[3] J.C. Fussell, M. Franklin, D.C. Green, M. Gustafsson, R.M. Harrison, W. Hicks, F.J. Kelly, F. Kishta, M.R. Miller, I.S. Mudway, F. Oroumiyeh, L. Selley, M. Wang, Y. Zhu, A review of road traffic-derived non-exhaust particles: emissions, physicochemical characteristics, health risks, and mitigation measures, Environ. Sci. Technol. 56 (2022) 6813–6835, https://doi.org/10.1021/acs.est.2c01072.
[4] A. Sinha, G. Ischia, C. Menapace, S. Gialanella, Experimental characterization protocols for wear products from disc brake materials, Atmosphere 11 (2020) 1102, https://doi.org/10.3390/atmos11101102.
[5] F. Amato, F.R. Cassee, H.A.C. Denier Van Der Gon, R. Gehrig, M. Gustafsson, W. Hafner, R.M. Harrison, M. Jozwicka, F.J. Kelly, T. Moreno, A.S.H. Prevot, M. Schaap, J. Sunyer, X. Querol, Urban air quality: the challenge of traffic non-exhaust emissions, J. Hazard Mater. 275 (2014) 31–36, https://doi.org/10.1016/j.jhazmat.2014.04.053.
[6] P. Peikertova, P. Filip, Influence of the automotive brake wear debris on the environment - a review of recent research, SAE Int. J. Mater. Manuf. 9 (2016) 133–146. https://www.jstor.org/stable/26268813.
[7] T. Gonet, B.A. Maher, J. Kukutschová, Source apportionment of magnetite particles in roadside airborne particulate matter, Sci. Total Environ. 752 (2021), 141828, https://doi.org/10.1016/j.scitotenv.2020.141828.
[8] D. Chan, G.W. Stachowiak, Review of automotive brake friction materials, Proc. Inst. Mech. Eng. - Part D J. Automob. Eng. 218 (2004) 953–966, https://doi.org/10.1243/0954407041856773.
[9] V.V. Kumar, S.S. Kumaran, Friction material composite: types of brake friction material formulations and effects of various ingredients on brake performance–a review, Mater. Res. Express 6 (2019), 082005, https://doi.org/10.1088/2053-1591/ab2404.
[10] S. Venkatesh, K. Murugapoopathiraja, Scoping review of brake friction material for automotive, Mater. Today: Proc. 16 (2019) 927–933, https://doi.org/10.1016/j.matpr.2019.05.178.
[11] P.V. Gurunath, J. Bijwe, Friction and wear studies on brake-pad materials based on newly developed resin, Wear 263 (2007) 1212–1219, https://doi.org/10.1016/j.wear.2006.12.050.
[12] S.J. Kim, M.H. Cho, D.-S. Lim, H. Jang, Synergistic effects of aramid pulp and potassium titanate whiskers in the automotive friction material, Wear 251 (2001) 1484–1491, https://doi.org/10.1016/S0043-1648(01)00802-X.
[13] S. Manoharan, G. Sai Krishnan, L. Ganesh Babu, V. R, D. Lenin Singaravelu, Synergistic effect of red mud-iron sulfide particles on fade-recovery characteristics of non-asbestos organic brake friction composites, Mater. Res. Express (2019), https://doi.org/10.1088/2053-1591/ab366f.
[14] G. Gautier Di Confiengo, M.G. Faga, Ecological transition in the Field of brake pad manufacturing: an overview of the potential green constituents, Sustainability 14 (2022) 2508, https://doi.org/10.3390/su14052508.
[15] P. Filip, Z. Weiss, D. Rafaja, On friction layer formation in polymer matrix composite materials for brake applications, Wear 252 (2002) 189–198, https://doi.org/10.1016/S0043-1648(01)00873-0.
[16] T. Gonet, B.A. Maher, I. Nyirő-Kósa, M. Pósfai, M. Vaculík, J. Kukutschová, Size-resolved, quantitative evaluation of the magnetic mineralogy of airborne brake-wear particulate emissions, Environ. Pollut. 288 (2021), 117808, https://doi.org/10.1016/j.envpol.2021.117808.
[17] J. Kukutschová, P. Moravec, V. Tomášek, V. Matějka, J. Smolík, J. Schwarz, J. Seidlerová, K. Šafářová, P. Filip, On airborne nano/micro-sized wear particles released from low-metallic automotive brakes, Environ. Pollut. 159 (2011) 998–1006, https://doi.org/10.1016/j.envpol.2010.11.036.
[18] M. Gasser, M. Riediker, L. Mueller, A. Perrenoud, F. Blank, P. Gehr, B. Rothen-Rutishauser, Toxic effects of brake wear particles on epithelial lung cells in vitro, Part. Fibre Toxicol. 6 (2009) 30, https://doi.org/10.1186/1743-8977-6-30.
[19] B. Apicella, A. Ciajolo, R. Barbella, A. Tregrossi, T.J. Morgan, A.A. Herod, R. Kandiyoti, Size exclusion chromatography of particulate produced in fuel-rich combustion of different fuels, Energy Fuels 17 (2003) 565–570, https://doi.org/10.1021/ef020149r.
[20] B. Apicella, R. Barbella, A. Ciajolo, A. Tregrossi, Comparative analysis of the structure of carbon materials relevant in combustion, Chemosphere 51 (2003) 1063–1069, https://doi.org/10.1016/S0045-6535(02)00715-4.
[21] Air Monitoring for Toxic Substances, Wiley & Sons, 2004.
[22] S. Rothenbacher, A. Messerer, G. Kasper, Fragmentation and bond strength of airborne diesel soot agglomerates, Part. Fibre Toxicol. 5 (2008) 9, https://doi.org/10.1186/1743-8977-5-9.
[23] W. Österle, A. Dmitriev, The role of solid lubricants for brake friction materials, Lubricants 4 (2016) 5, https://doi.org/10.3390/lubricants4010005.
[24] L. Lu, V. Sahajwalla, C. Kong, D. Harris, Quantitative X-ray diffraction analysis and its application to various coals, Carbon 39 (2001) 1821–1833, https://doi.org/10.1016/S0008-6223(00)00318-3.
[25] B. Manoj, A.G. Kunjomana, Study of stacking structure of amorphous carbon by X-ray diffraction technique, Int. J. Electrochem. Sci. 7 (2012) 3127–3134, https://doi.org/10.1016/S1452-3981(23)13940-X.
[26] C. Russo, A. Ciajolo, Effect of the flame environment on soot nanostructure inferred by Raman spectroscopy at different excitation wavelengths, Combust. Flame 162 (2015) 2431–2441, https://doi.org/10.1016/j.combustflame.2015.02.011.
[27] A.C. Ferrari, D.M. Basko, Raman spectroscopy as a versatile tool for studying the properties of graphene, Nat. Nanotechnol. 8 (2013) 235–246, https://doi.org/10.1038/nnano.2013.46.
[28] J. Kukutschová, V. Roubíček, M. Mašláň, D. Jančík, V. Slovák, K. Malachová, Z. Pavlíčková, P. Filip, Wear performance and wear debris of semimetallic automotive brake materials, Wear 268 (2010) 86–93, https://doi.org/10.1016/j.wear.2009.06.039.
[29] D.M. Agudelo-Castañeda, E.C. Teixeira, I.L. Schneider, S.R. Lara, L.F.O. Silva, Exposure to polycyclic aromatic hydrocarbons in atmospheric PM1.0 of urban environments: carcinogenic and mutagenic respiratory health risk by age groups, Environ. Pollut. 224 (2017) 158–170, https://doi.org/10.1016/j.envpol.2017.01.075.
[30] C. Russo, B. Apicella, A. Tregrossi, A. Ciajolo, K.C. Le, S. Török, P.-E. Bengtsson, Optical band gap analysis of soot and organic carbon in premixed ethylene flames: comparison of in-situ and ex-situ absorption measurements, Carbon 158 (2020) 89–96, https://doi.org/10.1016/j.carbon.2019.11.087.
[31] C. Russo, B. Apicella, A. Ciajolo, Blue and green luminescent carbon nanodots from controllable fuel-rich flame reactors, Sci. Rep. 9 (2019), 14566, https://doi.org/10.1038/s41598-019-50919-1.

[32] C. Russo, A. Carpentieri, A. Tregrossi, A. Ciajolo, B. Apicella, Blue, green and yellow carbon dots derived from pyrogenic carbon: structure and fluorescence behaviour, Carbon 201 (2023) 900–909, https://doi.org/10.1016/j.carbon.2022.09.062.
[33] B. Apicella, A. Ciajolo, A. Tregrossi, Fluorescence spectroscopy of complex aromatic mixtures, Anal. Chem. 76 (2004) 2138–2143, https://doi.org/10.1021/ac034860k.
[34] M. Alfè, B. Apicella, R. Barbella, A. Tregrossi, A. Ciajolo, Distribution of soot molecular weight/size along premixed flames as inferred by size exclusion chromatography, Energy Fuels 21 (2007) 136–140, https://doi.org/10.1021/ef060320p.
[35] C. Russo, A. Ciajolo, F. Stanzione, A. Tregrossi, B. Apicella, Separation and online optical characterization of fluorescent components of pyrogenic carbons for carbon dots identification, Carbon 209 (2023), 118009, https://doi.org/10.1016/j.carbon.2023.118009.
[36] S. Marcella, B. Apicella, A. Secondo, F. Palestra, G. Opromolla, R. Ciardi, V. Tedeschi, A.L. Ferrara, C. Russo, M. Rosaria Galdiero, L. Cristinziano, L. Modestino, G. Spadaro, A. Fiorelli, S. Loffredo, Size-based effects of anthropogenic ultrafine particles on activation of human lung macrophages, Environ. Int. 166 (2022), 107395, https://doi.org/10.1016/j.envint.2022.107395.